PCCP

The Mechanism of Fluidity Improvement of Cement Slurry by Graphene Oxide: A Study on Nanofriction

Journal:	*Physical Chemistry Chemical Physics*
Manuscript ID	CP-ART-11-2023-005374.R2
Article Type:	Paper
Date Submitted by the Author:	06-Mar-2024
Complete List of Authors:	Ji, Xiang; Qingdao University of Technology, Department of Civil Engineering Hou, Dongshuai; Qingdao University of Technology, Civil and Environmental Engineering Wang, Muhan; Qingdao University of Technology, Department of Civil Engineering Liu, Qing; Qingdao University of Technology, Department of Civil Engineering Hong, Fen; Qingdao University of Technology Wang, Yanshuai; Guangdong Province Key Laboratory of Durability for Marine Civil Engineering, The Key Laboratory on Durability of Civil Engineering in Shenzhen, Shenzhen University Fang, Guohao; Guangdong Province Key Laboratory of Durability for Marine Civil Engineering, The Key Laboratory on Durability of Civil Engineering in Shenzhen, Shenzhen University Hong, Shuxian; Guangdong Province Key Laboratory of Durability for Marine Civil Engineering, The Key Laboratory on Durability of Civil Engineering in Shenzhen, Shenzhen University Li, Mengmeng; Qingdao University of Technology, Department of Civil Engineering

The Mechanism of Fluidity Improvement of Cement Slurry by Graphene Oxide: A Study on Nanofriction

Xiang Ji[a], Dongshuai Hou[a], Muhan Wang[a], Liu Qing[a], Fen Hong[a], Yanshuai Wang[b], Guohao Fang[b], Shuxian Hong[b], Mengmeng Li[a,*]

a. Department of Civil Engineering, Qingdao University of Technology, Qingdao 266033, China;

b. College of Civil and Transportation Engineering, Guangdong Province Key Laboratory of Durability for Marine Civil Engineering, Shenzhen Key Laboratory for Low-carbon Construction Material and Technology, Shenzhen University, Shenzhen, China.

* Corresponding author, Mengmeng Li. Email: limengmeng7@126.com

ABSTRACT: Graphene oxide(GO) as a nano-reinforcing material has received extensive attention in cement composite materials. This paper employed molecular dynamics to simulate the friction process of calcium silicate hydrate (CSH) particles in the presence of double-sided and single-sided GCOOH (graphene oxide with a -COOH functional group, covering 10% of the surface). The investigation uncovered the lubricating effects of bifacial and unifacial GCOOH on the CSH interface. The findings indicate that the interfacial friction among CSH particles follows the sequence of double-sided GCOOH > pure CSH > single-sided GCOOH. In the double-sided GCOOH system, a greater external force is needed on the opposing side to alter the interaction with water molecules, calcium ions, and silica-oxygen tetrahedra, thereby enhancing friction. In contrast, the majority of the carboxyl groups on the single-sided GCOOH surface are strongly adsorbed onto the CSH surface, facilitating the entry of additional water molecules into the interlayer. Conversely, the unmodified side of the GCOOH has

lower interactions with water molecules, hence improving its lubricating properties.

Keywords: Graphene oxide; fluidity; Calcium Silicate Hydrate; Molecular Dynamics.

1 Introduction

Concrete is a crucial material used extensively in construction and infrastructure, and the mechanical properties of concrete play a vital role in ensuring the stability and durability of structures[1,2]. Researchers have been actively exploring different methods and materials to enhance the performance of concrete. Among these, carbon nanomaterials have garnered significant attention as a promising option to improve the mechanical properties of concrete due to their unique structure and exceptional performance[3,4]. Carbon nanomaterials, such as carbon fibers and carbon nanotubes, possess remarkable strength, stiffness, and electrical conductivity. By incorporating these nanomaterials into concrete, it becomes possible to enhance its mechanical properties and improve the overall structural quality[5–7]. The inclusion of carbon nanomaterials can augment the tensile strength, toughness, and durability of concrete, thereby enhancing its resistance to external loads and environmental factors.

GO is a carbon nanomaterial that is gaining popularity for its use in concrete[8–12]. It has a unique two-dimensional structure and excellent properties that can significantly improve the mechanical properties and functionality of concrete. The addition of GO can work in several ways to improve the quality of concrete. Firstly, it has a nanoscale flake structure that can fill microscopic defects in concrete, such as cracks and pores, thereby improving the denseness and reducing the porosity of the concrete[13–15]. This, in turn, enhances its mechanical properties and durability. Secondly, the addition of GO can reduce the penetration of water and harmful substances in concrete, thanks to its high specific surface area and barrier effect[16–19]. It prevents the penetration of water and gases while

reducing water absorption and chloride ion attack in concrete. This improves the water resistance and corrosion resistance of concrete. GO possesses excellent mechanical properties, including high strength and modulus, and exhibits a reinforcing effect[20–22]. When dispersed and uniformly introduced into concrete, GO can enhance its strength and stiffness. The interaction between GO and the concrete matrix effectively prevents the expansion of cracks, thereby increasing its tensile and flexural strength.

However, the mechanical performance of GO in concrete has sparked controversy. While Peng et al. [15,23,24] conducted experimental studies demonstrating that GO effectively enhances the compressive strength of concrete, Dimov's research[25] found that the addition of GO did not significantly improve the mechanical properties of concrete, failing to achieve the desired outcomes. Currently, there is no reasonable explanation for these contrasting results. An alternative perspective suggests that incorporating GO noticeably increases the viscosity of the cement paste, thereby reducing workability and impacting compressive strength[12,26,27]. Conversely, Qin et al. [28] discovered that the addition of GO at a dosage of 0.02% led to a significant increase in the fluidity of the cement paste. Different dosages of GO have varying effects on both the flowability and mechanical properties of concrete. It remains uncertain whether the influence of GO on strength affects flowability. Currently, despite several studies on the integration of nanomaterials like GO in concrete, there are still substantial study deficiencies in our comprehension of the molecular-level mechanisms that take place at the CSH-GO interface during shear. The specific mechanisms behind lubrication and friction, as well as the impact of alterations to functional groups on these interactions, remain incompletely investigated. The lack of understanding in this area is a significant obstacle to effectively using nanoparticles in concrete technology. In recent decades, the technology of and molecular dynamics (MD) simulations have been utilized for the examination of concrete materials[29–34], proving valuable in the exploration of the

characteristics of graphene oxide and oxide functionalized materials[35,36]. These studies have yielded useful knowledge about the behavior of nanomaterials in different situations and have established the basis for our research on the lubrication of the CSH-GO interface. . This technology has played a crucial role in understanding the nano-level information about the microstructure of cement-based materials. In a previous work[34], we conducted a molecular dynamics simulation to evaluate the fluidity of concrete and proposed an interfacial lubrication model. This model covers the complexity of cement hydrate interface interaction and can simulate the cement hydration process to a great extent. This study aims to clarify the fundamental mechanism of frictional contact between GO and CSH particles at the molecular scale. Simulations are employed to thoroughly examine the microstructural alterations and interaction dynamics that occur throughout the shearing process of the CSH-GO interface, thereby uncovering the intricate correlation between GO and CSH substrate movements. This study examines the impact of two-sided and one-sided functional group changes of GO on the interface of CSH. This work is unique because it thoroughly investigates the friction dynamics of the CSH-GO interface and how it improves the fluidity of cement paste. Through comprehending and capitalizing on these mechanisms, we have made a significant contribution to the progress of concrete technology by offering a fresh outlook on enhancing construction materials at the molecular scale.

2 Models and Simulation Details

2.1 Modelling Details

The 11Å tobermorite is a type of CSH mineral with a layered crystal structure[37–39]. The CSH configuration was simulated using a three-dimensional structure of 33.79Å×30.68Å×23.02Å, obtained by processing the 11Å tobermorite unit cell. The graphene model is derived from a single sheet of

graphite crystal with cell dimensions of 2.46 Å × 4.26 Å × 3.4 Å[40,41]. For the graphene simulation, a three-dimensional structure of 29.82Å×24.6Å×6.8Å was generated from the graphene unit cell. The surface of graphene was functionalized with carboxyl groups (-COOH) randomly terminated on the carbon atoms, covering both sides or one side of the graphene with 10% coverage. The coverage ratio may vary depending on the degree of oxidation, and the 10% coverage of groups falls within the range reported in the referenced publications for common surface-treated carbon fiber materials[40,42–44]. As shown in **Fig. 1c and Fig. 1d**, the interface configuration was prepared by sandwiching GO between two CSH sheets. In addition, 400 water molecules were randomly distributed in the interval. The number of water molecules is roughly converted from the density of pure water at one standard atmospheric pressure. The initial simulation box had dimensions of 33.79 Å × 30.68 Å × 100.57 Å in three dimensions. The height of 100.57 Å was chosen to minimize the impact of periodic boundaries on the upper and lower sheets.

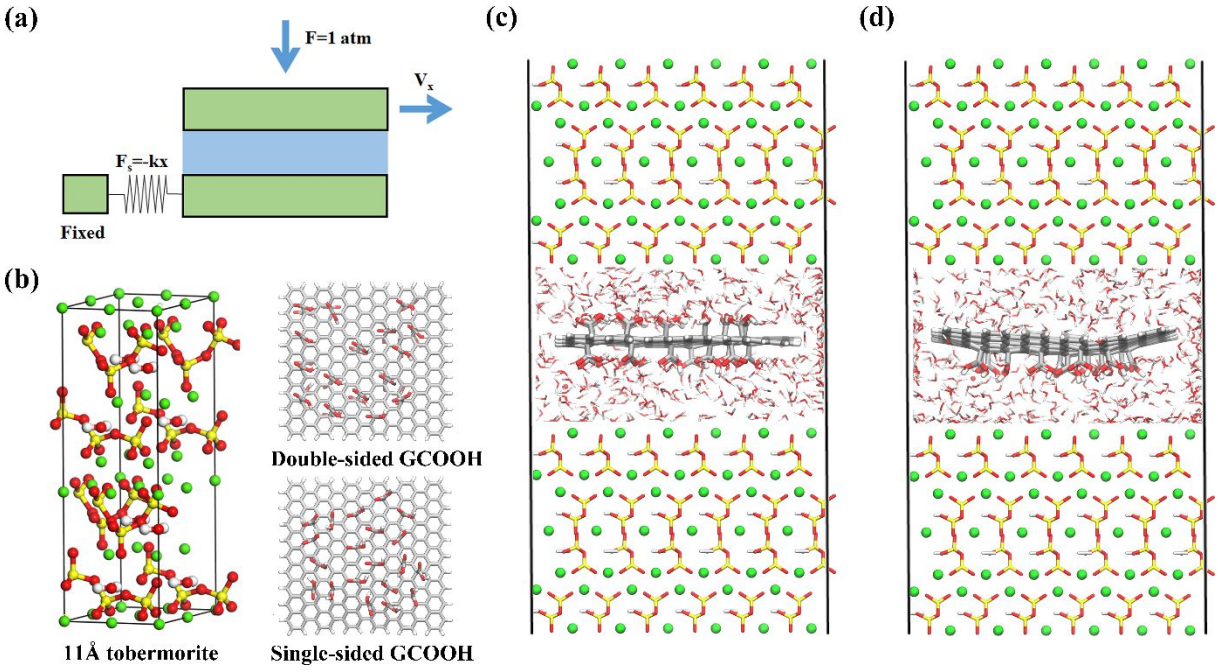

Fig. 1. (a) The geometry of the simulation system. The simulation system consists of solid sheets held together by a constant normal load F. The upper sheet moves at a constant velocity V_x, while the

substrate sheet is connected to a fixed stage through a spring with stiffness *k*. (b) The structures include the 11Å tobermorite cell structure, the double-sided graphene carboxyl (-GCOOH) model, and the single-sided -GCOOH model. (c)The 400 water molecules and the double-sided GCOOH are confined between two CSH sheets with a thickness of 20.23 Å. (d) The 400 water molecules and the single-sided GCOOH are confined between two CSH sheets with a thickness of 20.23 Å. The snapshots illustrate the identification of Ca, Si-O tetrahedron, water molecules, and -GCOOH, with color scheme representation as follows: red = oxygen, yellow = silicon, white = hydrogen, green = calcium, and gray = carbon.

In this simulation, the ReaxFF force field is employed to represent the non-bonding interactions among all atoms. Specifically, the all-atom (AA) model of the ReaxFF force field is utilized in the CSH model, which is commonly employed for investigating the hydration products of cementitious materials[45,46]. Within the reactive force field, the bond order is continually updated based on instantaneous atomic distances and local coordinate structures to accurately capture bond breakage and formation. This feature is particularly crucial for current modeling efforts involving chemical reactions between GO and CSH. Hou et al.[41,42] have successfully utilized the ReaxFF force field to construct a CSH surface model and investigate the interfacial reactions between GO and CSH, thus verifying the transferability and accuracy of the ReaxFF force field.

2.2 Equilibrium Molecular Dynamics Simulation

The MD simulations were performed using the Lammps software with the REAX package to incorporate the reaction force field. As shown in **Fig. 1a**, a suitable simulation model was constructed. The top part of the upper CSH sheet and the bottom part of the bottom CSH sheet (with a thickness of

4.08 Å) were defined as rigid bodies. The rigid body of the upper CSH sheet was subjected to a constant normal load of F = 1 atm, while the rigid body of the substrate CSH was fixed in the z-direction to achieve a standard atmospheric pressure state between the CSH sheets. The simulations were conducted under specific conditions, maintaining a temperature of 298 K. The resulting structures from these simulations were subsequently employed in the shear process.

2.3 Shear Process Simulation

The shear simulation is conducted using the final equilibrium configuration obtained from the equilibrium molecular dynamics simulation. In this shear process simulation, a constant velocity(V_x)is applied to the rigid body of the upper CSH. The movement of the upper rigid body drives the motion of the interlayer solution, leading to the displacement of the bottom CSH. As shown in **Fig. 1a**, the rigid body of the substrate CSH is connected to a fixed location through a spring with a stiffness value of k = 0.0007418 N/m. The expansion and contraction of the spring represent the frictional force experienced during the shearing of the substrate CSH.

The atomic trajectories in this simulation were integrated using the Verlet algorithm with a time step of 0.25 fs. The molecular dynamics simulations were conducted in the Hoover Canonical Ensemble (NVT) at a temperature of 298 K for a duration of 100 ps, where the temperature was controlled by a Nose-Hoover thermostat[47–49]. Visual Molecular Dynamics (VMD) software was utilized to visualize and display all snapshots obtained from the simulation[50].

3 Results and discussion

3.1 Microscale Lubrication of Water between CSH Sheets

Following the shear simulation, the temporal progression of the spring force acquired by the

simulation corresponds to the friction force across interfaces. This is illustrated in **Fig.2**, where the beginning curve of the CSH spring force is derived from a previously conducted lubrication model. Initially, the friction of all systems experiences a rapid increase followed by oscillations around a mean value. The graphic clearly illustrates that the initial friction peak is observed in all systems exhibiting shear motion of approximately 10 picoseconds. The relationship between the peak values is as follows: The double-sided GCOOH is superior to the original CSH but inferior to the single-sided GCOOH. Given the aforementioned phenomenon, a set of thought-provoking inquiries have emerged: What is the reason for the higher friction of the GO system when it interacts with functional groups on both sides, compared to the friction of the other two systems? What is the mechanism by which the presence of functional groups on one side of the GO system decreases the friction between sheets? The subsequent analysis will systematically address these crucial inquiries..

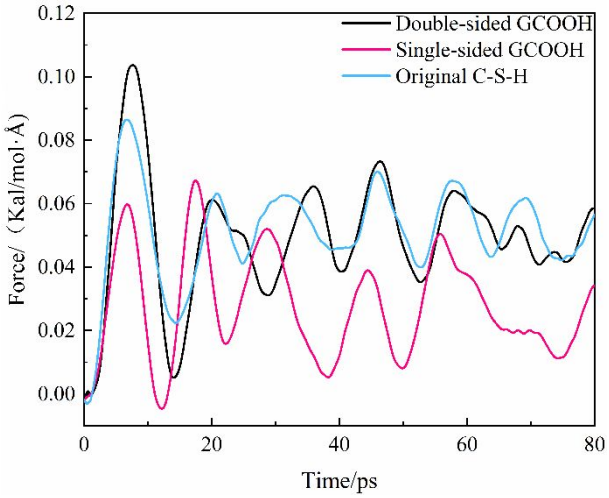

Fig. 2. Time evolution of the friction force of upper and substrate CSH sheets applied by the double-sided GCOOH, single-sided GCOOH, or non-GCOOH with 400 water molecules.

To gain a more intuitive understanding of the oscillation process, it is helpful to examine the temporal evolution configuration inside a single oscillation cycle, as shown in **Fig.3**. The initial configuration is formed through an equilibrium process, where the water molecules and GCOOH

molecules located between the CSH sheets reach a stable state under standard air pressure (as shown in **Fig.3a1 and 3b1**). The basal CSH plate's friction demonstrates elastic qualities in every cycle, as seen in **Fig.3a2 and 3b2**. The duration of the elastic phase may vary slightly due to variations in interlayer friction, but it does not surpass 15 picoseconds. **Fig.3a3 and 3b**3 demonstrate that the substrate CSH reaches its peak displacement and the friction begins to decline. In the double-sided GCOOH system, the substrate CSH experiences a greater maximum displacement compared to the single-sided GCOOH system. This is consistent with the observation that the peak frictional forces in the double-sided GCOOH system are significantly higher than those in the single-sided GCOOH system, as shown in **Fig.2**. Subsequently, the CSH substrate undergoes a reverse movement but fails to return to its initial position (as shown in **Fig.3a4 and 3b4**), initiating a new cycle of friction. Due to the increased friction in the double-sided GCOOH system, the substrate CSH moves further away from its initial position after reaching equilibrium. The observed phenomena are likely caused by the instability of the interaction between water molecules and GCOOH with substrate CSH. Additionally, the conformation of water molecules and GCOOH may alter between the two systems as shearing progresses. Therefore, a thorough examination is required to analyze the distribution of water molecules and GCOOH among the CSH sheets.

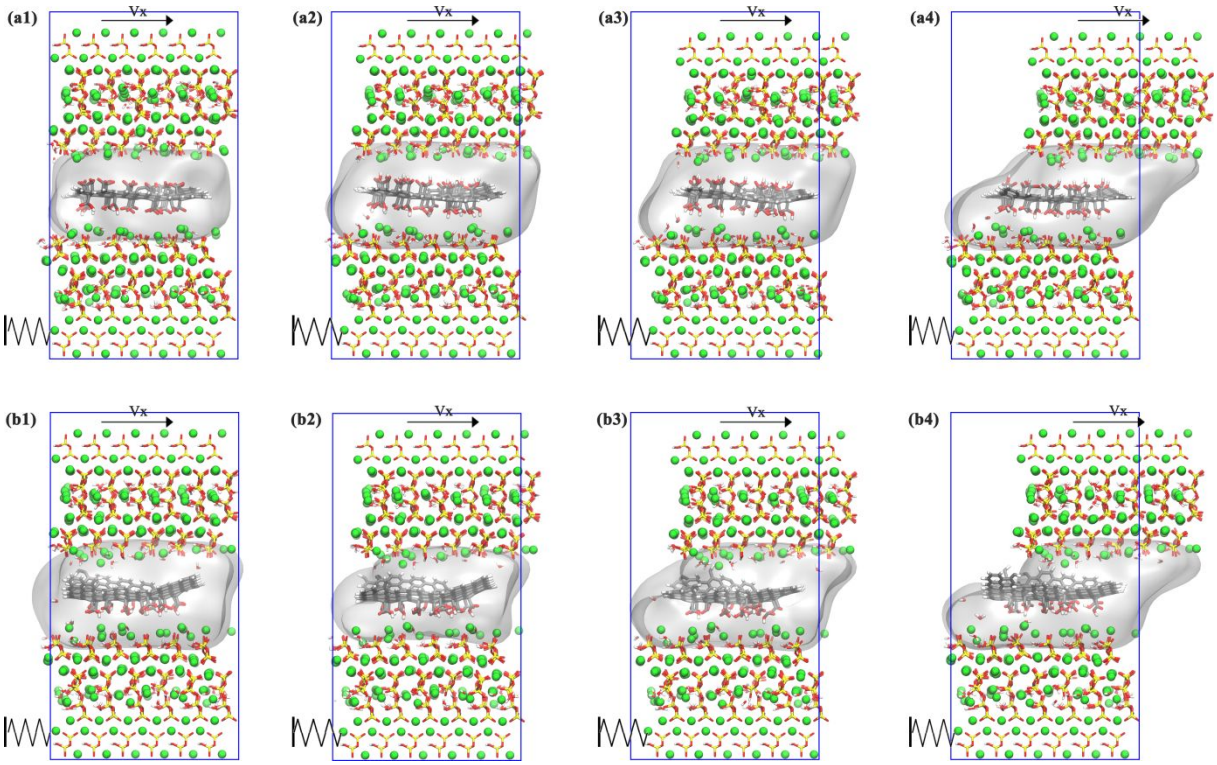

Fig. 3. The time evolution configuration of the double-sided GCOOH system during one oscillation period is as follows:(a1) Initial configuration, (a2) Elastic stage, (a3) Maximum displacement of the substrate CSH and (a4) Recovery stage. The time evolution configuration of the single-sided GCOOH system during one oscillation period is as follows:(b1) Initial configuration, (b2) Elastic stage, (b3) Maximum displacement of the substrate CSH and (b4) Recovery stage. The black vertical line represents the fixation phase, where a spring force is applied to the substrate CSH.

Fig.4 presents the computed density distribution curves of water molecules in both the double-sided GCOOH and single-sided GCOOH systems, allowing for the visualization of their distribution under equilibrium and shear conditions. Adsorption peaks are observed near the surfaces of both the upper and base CSH sheets, indicating a greater concentration of water molecules. The adsorption peak of the single-sided system on the CSH substrate surface exhibits a modest elevation in comparison to that of the double-sided system. However, the adsorption peak on the upper CSH surface is noticeably smaller in the single-sided system compared to the double-sided system. Furthermore, the application of shear diminishes the density distribution of water molecules on the substrate CSH surface, resulting in a minor release of water molecules. The density distribution of water molecules in pure CSH has a smooth form in the central region due to the absence of external structural influences on the water molecules located there.These data indicate that shear forces influence the adsorption of water molecules on the surface of CSH, and the presence of carboxyl groups modifies

the way CSH adsorbs water. To directly compare the distinctions between the equilibrium and shear configurations, we conducted additional research on the two-dimensional density distribution of water molecules within the CSH sheets.

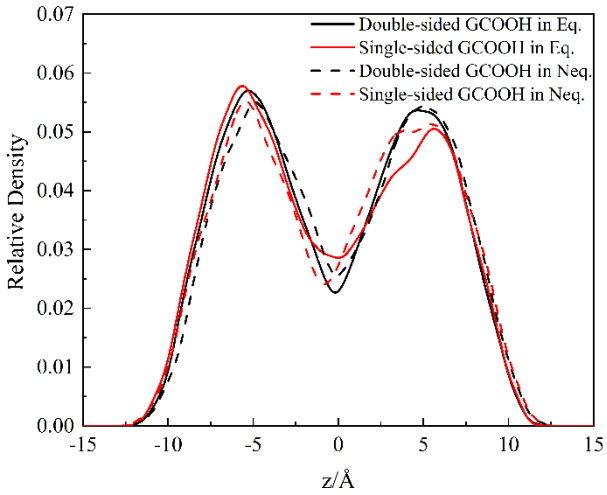

Fig. 4. The density profiles of water molecules in equilibrium and shear configuration.

The comparison of the two-dimensions density profiles of water molecules in the equilibrium and shear process is taken in **Fig. 5**. First of all, we can see the influence of the GCOOH configuration on the two-dimensional water distribution in the equilibrium configuration, as shown in **Fig. 5a1 and b1**. The double-sided GCOOH configuration is straight and can be in contact with water molecules to the greatest extent(as shown in **Fig. 5a3**). The single-sided GCOOH configuration is arched and the outer side of the arch is the side containing the functional group (as shown in **Fig. 5b3**). The arched shape makes the contact area between the functional group and water larger, which is more conducive to water adsorption. In the equilibrium state, the water distribution on the CSH side and the GCOOH side is uneven. During the equilibrium state, there is an unequal distribution of water between the CSH side and the GCOOH side. Furthermore, as shown in **Fig. 5a2 and 5b2**, the presence of shear leads to a more homogeneous dispersion of water molecules between CSH and GCOOH on the upper layer. However, there is no substantial alteration in the distribution of water molecules near the base CSH. The density profiles of water molecules undergo substantial changes under shearing action,

necessitating more investigation into the underlying mechanism.

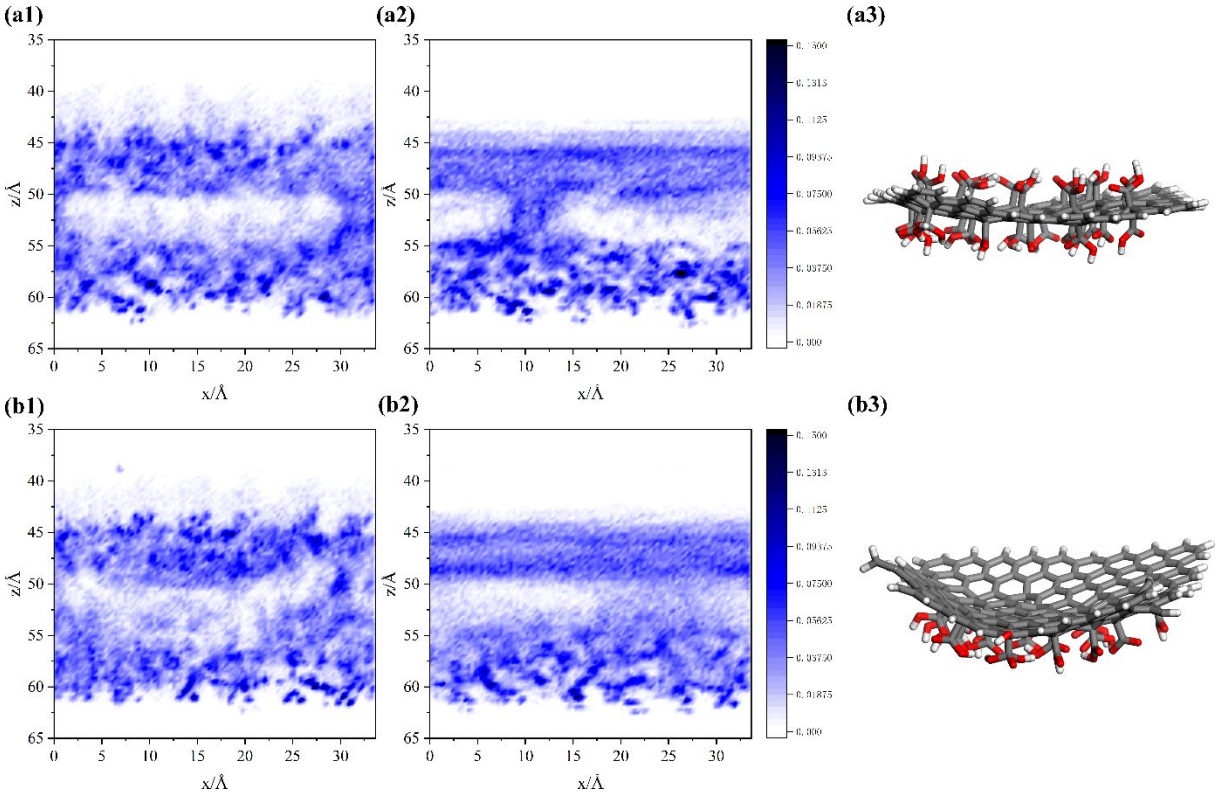

Fig. 5. The two-dimensions density profiles of water molecules between CSH sheets in (a1)equilibrium and (a2)shear configuration in the double-sided GCOOH system, and in (b1)equilibrium and (b2)shear configuration in the single-sided GCOOH system, respectively. The configuration of (a3)double-sided GCOOH and (b3)single-sided GCOOH in shear progress.

In summary of **Fig. 2 to 5**, the microstructure of water distribution and GCOOH in the double-sided GCOOH and single-sided GOOH system is different, which is the main factor that affects the interfacial friction. The changes in the microstructure are attributed to the interactions between molecules. Therefore, the interface interaction mechanism between CSH sheets with double-sided and single-sided GCOOH is analyzed from two parts: microstructure analysis and intermolecular interaction analysis. Subsequently, we will elucidate the alterations in the microstructure following the application of shear and identify the pivotal molecular interactions involved in the shearing process.

3.2 Microscopic Origin of Interfacial Lubrication

The distribution of the order parameter (Sm) in the equilibrium and shear configuration is calculated to quantitatively evaluate the impact of an aqueous environment on the microstructure of water molecules. The order parameter is a crucial parameter for assessing the molecular arrangement and aggregation structure, and it is expressed as follows:

$$S_m = \frac{1}{2}\langle 3cos^2 2\beta - 1\rangle \quad (1)$$

In the equation, β represents the angle between two orientations of the water dipole. A value of Sm approaching 1 indicates a high order, while a value of Sm approaching -0.5 indicates a low order.

As shown in **Fig. 6a**, the low-order parameters of the water molecules of the two systems are not much different in the equilibrium state, but the value of the high-order water is much larger than that in the shearing state. Under the shearing action, the value of the high-order water of the double-sided system is significantly reduced. This phenomenon shows that the shearing action has a certain influence on the microstructure of water aggregation and the interaction between water and water in the double-GCOOH system. The directional distribution of water molecule dipoles is affected by shearing, as shown in **Fig. 6b and 6c**, which are concentrated at 0° and 180°. The direction of 0° and 180° represents the adsorbed water on the upper CSH surface, substrate CSH surface, or GCOOH surface. In the previous work, the shearing action destroyed the adsorption of water molecules on the CSH surface, which reduced the dipole angle distribution in the 0° and 180° directions. However, in these two systems, the dipole angle distribution in the 0° and 180° directions increases, which means that the shearing action also destroys the water molecules adsorbed on the GCOOH surface.

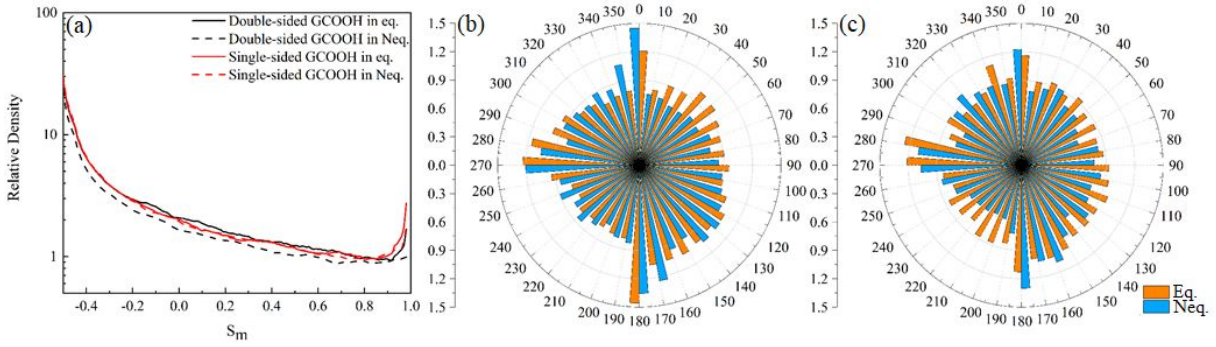

Fig. 6. The distribution of water order parameters between CSH sheets (a) in the equilibrium and shear progress of the double-sided GCOOH system and the single-sided GCOOH system.The distribution of dipole direction of water molecules (b) in the equilibrium and shear configuration of the double-sided GCOOH system and (c) the single-sided GCOOH system

During the shearing process, not only the interaction between the interface and the water molecules is affected, but what other interactions produce changes? The constant change of friction during the shearing process means that the interaction between the molecules is constantly changing. The radial distribution function (RDF) is defined as the ratio of the local density to the average density. We usually use RDF to characterize the strength of the interaction between atoms. The RDF between the relevant pairs of water-Ca,water-SiO tetrahedron, water-COOH, COOH-Ca, COOH-SiO tetrahedron, Water-C, and Ca-SiO tetrahedron, was calculated during the shearing process(as shown in **Fig. 7)**. The above seven sets of interactions correspond to four parts of the interface interaction: water desorbed from the CSH surface or GCOOH surface, GCOOH or Ca separated from the CSH substrate.

The RDF between the water and Ca ions and between the water and SiO tetrahedron has an obvious peak around 1 Å and 2.35 Å, respectively, and the RDF peak in the double-sided GCOOH system is higher than that of the single-sided GCOOH system(as shown in **Fig. 7a**). This phenomenon occurs because the single-sided GCOOH system only adsorbs water on the side with a higher concentration

of carboxyl groups at the same coverage. Furthermore, a significant portion of the carboxyl groups with the CSH surface for water molecules. As a result, the water molecules adsorbed on the CSH surface have a higher tendency to desorb. The interaction of GCOOH with CSH in cementitious systems with carboxyl functionality is an important component of our research since it helps us understand the mechanism behind the enhancement of cement paste fluidity. As shown in **Fig. 7b**, the first peaks of RDFs in both Ocooh-Ca and Ocooh-Osio pairs in single-sided GCOOH system are higher than those in double-sided GCOOH system, and the position of the first peak in single-sided GCOOH system is closer to CSH surface, indicating that GCOOH in single-sided GCOOH system is more likely to be adsorbed on CSH surface. In addition, by comparing the RDF of Ca-SiO tetrahedron and water-C(up) and water-COOH(up) in **Fig. 7c**, it can be observed that the peak value of the double-sided GCOOH system is much higher than that of the single-sided GCOOH system, and the peak of the Ca and O_{cooh} bond is higher in the double-sided GCOOH system. Based on the above facts, we can infer that it is difficult for water molecules to act on single-sided GCOOH, and the interaction between double-sided GCOOH and water is stronger, and double-sided GCOOH can enhance the Ca-SiO tetrahedral interaction, thereby inhibiting the move of Ca ions from the CSH substrate.

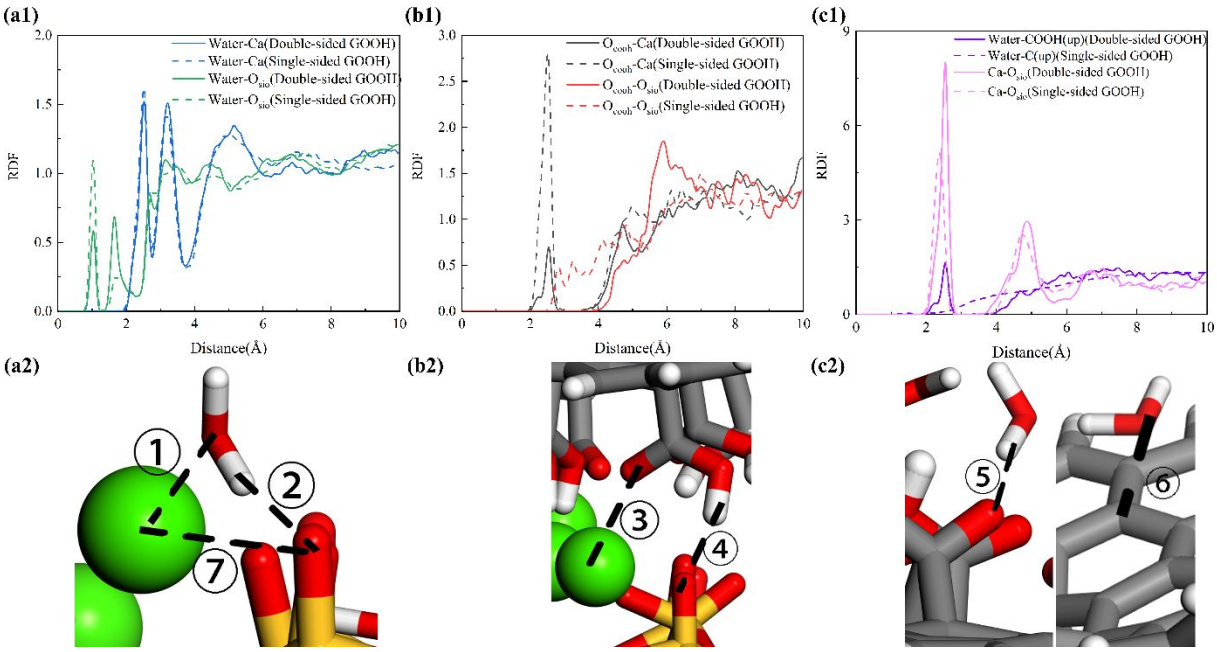

Fig. 7. Radial distribution function (RDF) in the shearing process of the noncovalent pairs of (a1) ① Water-COOH, ②Water-SiO tetrahedron, (b2) ③COOH-Ca, ④COOH-SiO tetrahedron and (c3)⑤ Water-COOH(up), ⑥Water-C(up), ⑦Ca-SiO tetrahedron.

The strength and stability of molecular and ionic bonds can be quantitatively described using the Time Correlation Function (TCF). The TCF for noncovalent bonds is calculated using the following formula:

$$C\ (t)\ = \frac{< \delta b(t)\delta b(0) >}{\delta b(0)\delta b(0)} \quad (2)$$

Where the δb(t) is a binary operator. The δb(t) equals 1 if the noncovalent bond is generated, otherwise equals 0.

As shown in **Fig. 8**, the TCF of the Water-Ca pair decreases significantly, but the double-sided system decreases more slowly and the final stable value is also higher, which indicates that the interaction of the non-covalent Water-Ca pair in the system is a bit more stable and is relatively less affected by the shearing effect. The TCF of the COOH-Ca pair in the two-sided system stays above

0.9, and that of the COOH-Ca pair in the one-sided system stays at 0.8, which proves that the carboxyl group interaction with the Ca ions on the surface of CSH is not easy to be broken under shear and that the stability of the COOH-Ca bond is much better in the double-sided GCOOH system so that more external force is needed for the double-sided GCOOH to be detached from the surface of CSH. **Fig. 9** shows the time evolution of relative (non)covalent bond contents of Ca-SiO tetrahedron, Water-SiO tetrahedron, and Water-COOH in two systems, where the bond time evolution is a parameter used to estimate the change in the content of molecular or atomic interaction bonds. Firstly, the variation of Ca-SiO tetrahedron bonding content in the double-sided GCOOH system is smaller than that in the single-sided GCOOH system, which indicates that the interaction between Ca and SiO tetrahedra in this system is relatively stable and difficult to be broken under shear. Secondly, the bonding content of water-SiO tetrahedra fluctuates greatly in the two systems, and most of the values are lower than 1.0, which can be inferred that the water molecules adsorbed on the surface of SiO tetrahedra are destroyed during the shear process, and the GCOOH weakens the water-absorbing ability of SiO tetrahedra. Finally, the bonding content of Water-COOH also fluctuates considerably. The overall bonding content of the double-sided GCOOH system shows an increasing trend, while the overall bonding content of the single-sided GCOOH system shows a decreasing trend. This phenomenon also proves that the GCOOH with modified functional groups on both sides has a significantly stronger ability to compete for water molecules than the GCOOH with modified functional groups on one side. Increased adsorption of water molecules leads to a decrease in the presence of freely moving water molecules between sheets, resulting in a reduction of the interfacial lubrication effect.

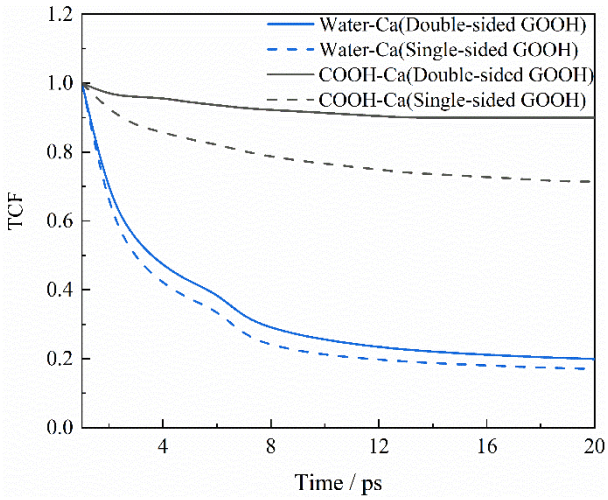

Fig. 8. Time correlation function (TCF) of the noncovalent pairs of Water-Ca and COOH-Ca.

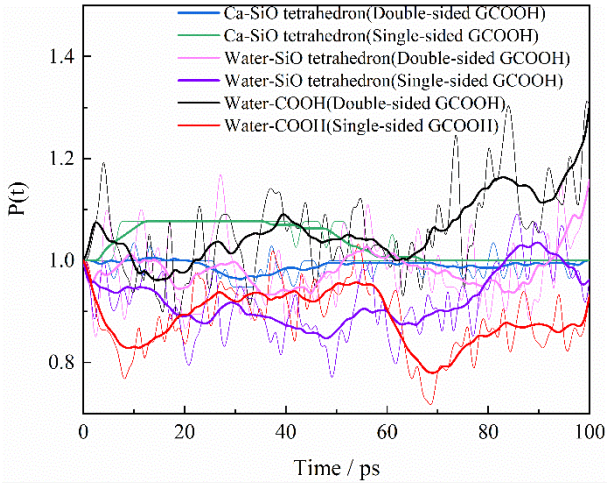

Fig. 9. Time evolution of bonding (BTE) of the noncovalent pairs of Ca- SiO tetrahedron, Water- SiO tetrahedron, and Water-COOH in double-sided GCOOH and single-sided GCOOH systems. The dotted line is the original data, and the solid line is the trend line.

As previously stated, the double-sided GCOOH adheres more securely to the CSH surface, and the carboxyl groups on the upper surface have a stronger interaction with water molecules, resulting in increased friction at the GCOOH/CSH contact. The majority of the adsorption sites on the substrate's CSH surface are taken up by one-sided GCOOH, causing more water molecules to detach from the CSH surface and contribute to interlayer lubrication. As a result, the interaction between the water

molecules and the C-atoms of the one-sided GCOOH becomes less strong, leading to a decrease in interfacial friction.

3.3 Discussion of Mode of Action

These different modes of action between single-sided and double-sided GO can lead to variations in their effects on the properties and behavior of CSH in concrete systems. Double-sided GO has an increased friction capacity in cement particles. It offers two functionalized surfaces, allowing for stronger and more extensive adsorption of water molecules on both sides of the CSH surface. With functional groups present on both sides, double-sided GO has a higher potential for interaction with the CSH surface compared to single-sided GO. The insertion of single-sided GO between CSH sheets can act as a lubricant, reducing friction and enabling easier sliding or movement between the CSH sheets. It primarily interacts with the CSH surface through the adsorption of its functional groups, such as carboxyl groups, onto the CSH surface. The groups on single-sided GO can compete with the CSH surface for water molecules, potentially leading to the desorption of water molecules from the CSH surface. As single-sided GO only has functional groups on one side, its interaction with the CSH surface is limited to that side. The carbon atoms on the unaltered side of the single-sided GO exhibit minimal affinity towards water molecules and the upper CSH interface. Instead, they facilitate lubrication with other ions or molecules present in the cement paste.For designing GO, double-sided GO exhibits higher adsorption capability, leading to enhanced mechanical properties of concrete. On the other hand, single-sided GO demonstrates greater lubrication performance, enhancing the fluidity of concrete.

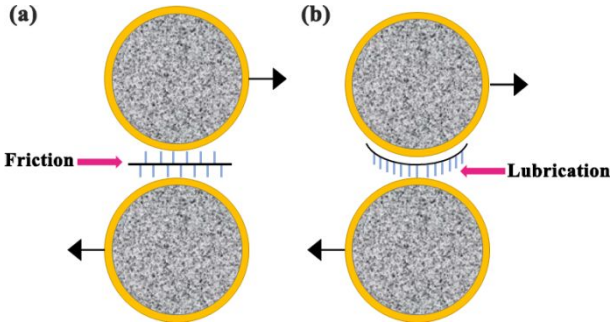

Fig. 10. The comparison of modes of action between double-sided GCOOH and single-sided GCOOH in concrete systems.

4 Conclusion

In this study, we employed molecular dynamics simulations to investigate the interface friction between CSH and GO sheets. Through shear MD simulations, we observed the microscopic enhancement behavior and examined the changes in microstructural parameters during the shearing process. Our results revealed the strong correlation between GO and the movement of the CSH substrate, providing insights into the lubrication effect of both double-sided and single-sided modified functional group GO at the CSH interface. Furthermore, our investigations on the friction between GO and the CSH substrate demonstrated the redistribution of water molecules between the sheets induced by the shearing effect. The double-sided GCOOH system has a lower density of functional groups and occupies fewer adsorption sites on the CSH surface, facilitating the interaction between water molecules and the CSH substrate. Conversely, the functional groups on the other side exhibit stronger interaction with water molecules and require a higher external force to disrupt the interaction between water molecules and the CSH interface or carboxyl groups. The observed increase in friction between GO and CSH, modified with functional groups on both sides, is considered to be the underlying mechanism responsible for the enhanced mechanical properties of concrete achieved by GO. Based on

the investigation of the single-sided GCOOH system, it is deduced that a significant portion of the carboxyl groups on one side of GCOOH are firmly adsorbed onto the CSH surface. This adhesion allows for a greater number of water molecules to interact and provide lubrication at the interface. Conversely, the unmodified side of GCOOH lacks interaction with water molecules, suggesting that the adsorption of one-sided GCOOH optimizes the CSH surface and mitigates friction at the micro-interface to some extent. Consequently, the presence of single-sided GCOOH proves advantageous in enhancing the fluidity of cement slurry.

This study offers a potential avenue for comprehending the mechanism underlying single-sided or double-sided functionalization of GO in CSH. Future investigations should focus on identifying the specific types of functional groups modified on the surface of GO and determining if there exists an optimal coverage of functional groups that can effectively reduce friction between CSH particles after the incorporation of GO. Unveiling these mechanisms will enhance the theoretical foundation of GO-cement composites and facilitate the optimization of their properties. Consequently, graphene-reinforced concrete holds great promise as a promising material.

CRediT authorship contribution statement

Xiang Ji: Data curation, Formal analysis, Investigation,Methodology, Visualization, Writing - original draft **Liu Qing:** Formal analysis, Writing – original draft. **Dongshuai Hou:** Data curation, Methodology, Software, Visualization, Writing – review & editing. **Muhan Wang:** Funding acquisition, Investigation, Writing – review & editing. **Fen Hong:** Investigation, Resources. Muhan Wang: Supervision, Visualization. **YanShuai Wang:** Supervision, Visualization. **Guohao Fang:** Supervision, Visualization. **Shuxian Hong:** Supervision, Visualization. **Mengmeng Li:** Data curation, Methodology, Validation.

Declaration of Competing Interest

The authors declare that they have no known competing financial interests or personal relationships that could have appeared to influence the work reported in this paper.

Acknowledgment

M. W. and D. H. financial support from the National Natural Science Foundation of China under Grant U2006224, 51978352, 51908308, 52178221, National Key Research and Development project 2022YFE0133800， Natural Science Foundation of Shandong Province under Grant ZR2020QE253, ZR2020JQ25, Shandong Provincial Education Department under Grant 2019KJG010, Qingdao Research Program 16-5-1-96-jch, 111 Project TMduracon20220022.

References

1 F. Qu, W. Li, W. Dong, V. W. Y. Tam and T. Yu, Durability deterioration of concrete under marine environment from material to structure: A critical review, *J. Build. Eng.*, 2021, **35**, 102074.

2 R. O'Hegarty, O. Kinnane, J. Newell and R. West, High performance, low carbon concrete for building cladding applications, *J. Build. Eng.*, 2021, **43**, 102566.

3 Y. Du, J. Yang, B. Skariah Thomas, L. Li, H. Li, W. Mohamed Shaban and W. Tung Chong, Influence of hybrid graphene oxide/carbon nanotubes on the mechanical properties and microstructure of magnesium potassium phosphate cement paste, *Constr. Build. Mater.*, 2020, **260**, 120449.

4 M. Du, H. Jing, Y. Gao, H. Su and H. Fang, Carbon nanomaterials enhanced cement-based composites: Advances and challenges, *Nanotechnol. Rev.*, 2020, **9**, 115–135.

5 S. Baban Singh, Sbv. Raj and F. Year, 66 IJSR-INTERNATIONAL JOURNAL OF SCIENTIFIC RESEARCH Effect of Multiwalled Carbon Nanotubes On Mechanical

Properties of Concrete Surajit Paul, 2013, 2–4.

6 S. P. Shah, P. Hou and M. S. Konsta-Gdoutos, Nano-modification of cementitious material: Toward a stronger and durable concrete, *J. Sustain. Cem. Mater.*, 2015, **5**, 1–22.

7 P. Zhang, J. Su, J. Guo and S. Hu, Influence of carbon nanotube on properties of concrete: A review, *Constr. Build. Mater.*, 2023, **369**, 130388.

8 A. Habibnejad Korayem, P. Ghoddousi, A. A. Shirzadi Javid, M. A. Oraie and H. Ashegh, Graphene oxide for surface treatment of concrete: A novel method to protect concrete, *Constr. Build. Mater.*, 2020, **243**, 118229.

9 P. K. Akarsh, D. Shrinidhi, S. Marathe and A. K. Bhat, Graphene oxide as nano-material in developing sustainable concrete – A brief review, *Mater. Today Proc.*, 2022, **60**, 234–246.

10 S. C. Devi and R. A. Khan, Effect of graphene oxide on mechanical and durability performance of concrete, *J. Build. Eng.*, 2020, **27**, 101007.

11 S. Chuah, Z. Pan, J. G. Sanjayan, C. M. Wang and W. H. Duan, Nano reinforced cement and concrete composites and new perspective from graphene oxide, *Constr. Build. Mater.*, 2014, **73**, 113–124.

12 L. Lu and D. Ouyang, Properties of cement mortar and ultra-high strength concrete incorporating graphene oxide nanosheets, *Nanomaterials*, 2017, **7**, 1–14.

13 K. Chintalapudi and R. M. R. Pannem, An intense review on the performance of Graphene Oxide and reduced Graphene Oxide in an admixed cement system, *Constr. Build. Mater.*, 2020, **259**, 120598.

14 L. Zhao, X. Guo, L. Song, Y. Song, G. Dai and J. Liu, An intensive review on the role of graphene oxide in cement-based materials, *Constr. Build. Mater.*, 2020, **241**, 117939.

15 H. Peng, Y. Ge, C. S. Cai, Y. Zhang and Z. Liu, Mechanical properties and microstructure of graphene oxide cement-based composites, *Constr. Build. Mater.*, 2019, **194**, 102–109.

16 C. S. R. Indukuri and R. Nerella, Enhanced transport properties of graphene oxide based cement composite material, *J. Build. Eng.*, , DOI:10.1016/j.jobe.2021.102174.

17 H. Zeng, S. Qu and Y. Qin, Microstructure and transport properties of cement-based material enhanced by graphene oxide, *Mag. Concr. Res.*, 2021, **73**, 1011–1024.

18 H. Du, H. J. Gao and S. D. Pang, Improvement in concrete resistance against water and chloride ingress by adding graphene nanoplatelet, *Cem. Concr. Res.*, 2016, **83**, 114–123.

19 A. Mohammed, J. G. Sanjayan, W. H. Duan and A. Nazari, Incorporating graphene oxide in cement composites: A study of transport properties, *Constr. Build. Mater.*, 2015, **84**, 341–347.

20 K. Chintalapudi and R. M. R. Pannem, Strength properties of graphene oxide cement composites, *Mater. Today Proc.*, 2019, **45**, 3971–3975.

21 Z. Pan, L. He, L. Qiu, A. H. Korayem, G. Li, J. W. Zhu, F. Collins, D. Li, W. H. Duan and M. C. Wang, Mechanical properties and microstructure of a graphene oxide-cement composite, *Cem. Concr. Compos.*, 2015, **58**, 140–147.

22 F. Babak, H. Abolfazl, R. Alimorad and G. Parviz, Preparation and mechanical properties of graphene oxide: Cement nanocomposites, *Sci. World J.*, , DOI:10.1155/2014/276323.

23 H. Sun, L. Ling, Z. Ren, S. A. Memon and F. Xing, Effect of graphene oxide/graphene hybrid on mechanical properties of cement mortar and mechanism investigation, *Nanomaterials*, , DOI:10.3390/nano10010113.

24 G. Jing, J. Wu, T. Lei, S. Wang, V. Strokova, V. Nelyubova, M. Wang and Z. Ye, From graphene oxide to reduced graphene oxide: Enhanced hydration and compressive strength of cement composites, *Constr. Build. Mater.*, 2020, **248**, 118699.

25 D. Dimov, I. Amit, O. Gorrie, M. D. Barnes, N. J. Townsend, A. I. S. Neves, F. Withers, S. Russo and M. F. Craciun, Ultrahigh Performance Nanoengineered Graphene–Concrete Composites for Multifunctional Applications, *Adv. Funct. Mater.*, , DOI:10.1002/adfm.201705183.

26 Q. Wang, X. Cui, J. Wang, S. Li, C. Lv and Y. Dong, Effect of fly ash on rheological properties of graphene oxide cement paste, *Constr. Build. Mater.*, 2017, **138**, 35–44.

27 X. Liu and Y. Li, Plain Concrete Prisms Externally Strengthened by CFRP Bonded with

Graphene Oxide–Modified Magnesium Phosphate Cement, *J. Mater. Civ. Eng.*, 2020, **32**, 1–9.

28 Q. Wang, J. Wang, C. X. Lu, B. W. Liu, K. Zhang and C. Z. Li, Influence of graphene oxide additions on the microstructure and mechanical strength of cement, *Xinxing Tan Cailiao/New Carbon Mater.*, 2015, **30**, 349–356.

29 D. Hou, X. Ji, P. Wang, J. Zhang and M. Wang, Atypical adsorption of polycarboxylate superplasticizers on calcium silicate hydrate surface: Converting interaction by solvent effects, *Constr. Build. Mater.*, 2022, **330**, 127160.

30 D. Tavakoli and A. Tarighat, Molecular dynamics study on the mechanical properties of Portland cement clinker phases, *Comput. Mater. Sci.*, 2016, **119**, 65–73.

31 D. Lau, W. Jian, Z. Yu and D. Hui, Nano-engineering of construction materials using molecular dynamics simulations: Prospects and challenges, *Compos. Part B Eng.*, 2018, **143**, 282–291.

32 D. Hou, Q. Yang, Z. Jin, P. Wang, M. Wang, X. Wang and Y. Zhang, Enhancing interfacial bonding between epoxy and CSH using graphene oxide: An atomistic investigation, *Appl. Surf. Sci.*, 2021, **568**, 150896.

33 D. Hou, H. Zheng, P. Wang, X. Wan, B. Yin, M. Wang and J. Zhang, Molecular dynamics study on sodium chloride solution transport through the Calcium-Silicate-Hydrate nanocone channel, *Constr. Build. Mater.*, 2022, **342**, 128068.

34 M. Wang, K. Zhang, X. Ji, P. Wang, H. Ma, J. Zhang and D. Hou, Molecular insight into the fluidity of cement pastes: Nano-boundary lubrication of cementitious materials, *Constr. Build. Mater.*, 2022, **316**, 125800.

35 A. Verma and A. Parashar, Reactive force field based atomistic simulations to study fracture toughness of bicrystalline graphene functionalised with oxide groups, *Diam. Relat. Mater.*, 2018, **88**, 193–203.

36 A. Verma and A. Parashar, Molecular dynamics based simulations to study the fracture strength of monolayer graphene oxide, *Nanotechnology.*, 2018, **29(11)**,. 115706.

37 S. Merlino, E. Bonaccorsi and T. Armbruster, The real structure of tobermorite 11A: normal and anomalous forms, OD character and polytypic modifications, *Eur. J. Mineral.*, 2001, **13**, 577–590.

38 R. J. Kirkpartick, J. L. Yarger, P. F. McMillan, P. Yu and X. Cong, Raman spectroscopy of C-S-H, tobermorite, and jennite, *Adv. Cem. Based Mater.*, 1997, **5**, 93–99.

39 S. A. Hamid, Crystal structure of the 11 Å natural tobermorite $Ca_{2.25}[Si_3O_{7.5}(OH)_{1.5}].1H_2O$, *Zeitschrift für Krist.*, 1981, **154**, 189–198.

40 F. Sanchez and L. Zhang, Molecular dynamics modeling of the interface between surface functionalized graphitic structures and calcium-silicate-hydrate: Interaction energies, structure, and dynamics, *J. Colloid Interface Sci.*, 2008, **323**, 349–358.

41 D. Hou, T. Yang, J. Tang and S. Li, Reactive force-field molecular dynamics study on graphene oxide reinforced cement composite: Functional group de-protonation, interfacial bonding and strengthening mechanism, *Phys. Chem. Chem. Phys.*, 2018, **20**, 8773–8789.

42 D. Hou, Z. Lu, X. Li, H. Ma and Z. Li, Reactive molecular dynamics and experimental study of graphene-cement composites: Structure, dynamics and reinforcement mechanisms, *Carbon N. Y.*, 2017, **115**, 188–208.

43 M. A. Montes-Morán, F. W. J. Van Hattum, J. P. Nunes, A. Martínez-Alonso, J. M. D. Tascón and C. A. Bernardo, A study of the effect of plasma treatment on the interfacial properties of carbon fibre-thermoplastic composites [6], *Carbon N. Y.*, 2005, **43**, 1795–1799.

44 R. D. Allington, D. Attwood, I. Hamerton, J. N. Hay and B. J. Howlin, A model of the surface of oxidatively treated carbon fibre based on calculations of adsorption interactions with small molecules, *Compos. Part A Appl. Sci. Manuf.*, 1998, **29**, 1283–1290.

45 D. Hou, T. Zhao, H. Ma and Z. Li, Reactive molecular simulation on water confined in the nanopores of the calcium silicate hydrate gel: Structure, Reactivity, and mechanical properties, *J. Phys. Chem. C*, 2015, **119**, 1346–1358.

46 H. Manzano, E. Masoero, I. Lopez-Arbeloa and H. M. Jennings, Shear deformations in

calcium silicate hydrates, *Soft Matter*, 2013, **9**, 7333–7341.

47 M. Bauchy, H. Laubie, M. J. Abdolhosseini Qomi, C. G. Hoover, F. J. Ulm and R. J. M. Pellenq, Fracture toughness of calcium-silicate-hydrate from molecular dynamics simulations, *J. Non. Cryst. Solids*, 2015, **419**, 58–64.

48 S. Nosé, Molecular Physics: An International Journal at the Interface Between Chemistry and Physics A molecular dynamics method for simulations in the canonical ensemble A molecular dynamics method for simulations in the canonical ensemblet, *An Int. J. Interface Between Chem. Phys. Mol. Phys.*, 1984, **52**, 255–268.

49 Y. Kassir, M. Kupiec, A. Shalom and G. Simchen, Cloning and mapping of CDC40, a Saccharomyces cerevisiae gene with a role in DNA repair, *Curr. Genet.*, 1985, **9**, 253–257.

50 W. Humphrey, A. Dalke and K. Schulten, VMD : Visual Molecular Dynamics, 1996, **7855**, 33–38.